Molecular mechanisms underlying the effect of the novel BK channel opener GoSlo: Involvement of the S4/S5 linker and the S6 segment

Timothy I. Webb[a,1], Aravind Singh Kshatri[b,1], Roddy J. Large[a], Adebola Morayo Akande[b], Subhrangsu Roy[a], Gerard P. Sergeant[a,b], Noel G. McHale[a,b], Keith D. Thornbury[a,b], and Mark A. Hollywood[a,b,2]

[a]Ion Channel Biotechnology Centre and [b]The Smooth Muscle Research Centre, Dundalk Institute of Technology, Dundalk, County Louth, Ireland

Edited* by Richard W. Aldrich, The University of Texas at Austin, Austin, TX, and approved January 5, 2015 (received for review January 15, 2014)

GoSlo-SR-5-6 is a novel large-conductance Ca^{2+}-activated K^+ (BK) channel agonist that shifts the activation $V_{1/2}$ of these channels in excess of −100 mV when applied at a concentration of 10 μM. Although the structure–activity relationship of this family of molecules has been established, little is known about how they open BK channels. To help address this, we used a combination of electrophysiology, mutagenesis, and mathematical modeling to investigate the molecular mechanisms underlying the effect of GoSlo-SR-5-6. Our data demonstrate that the effects of this agonist are practically abolished when three point mutations are made: L227A in the S4/S5 linker in combination with S317R and I326A in the S6C region. Our data suggest that GoSlo-SR-5-6 interacts with the transmembrane domain of the channel to enhance pore opening. The Horrigan–Aldrich model suggests that GoSlo-SR-5-6 works by stabilizing the open conformation of the channel and the activated state of the voltage sensors, yet decouples the voltage sensors from the pore gate.

ion channels | modulators | structure function

Large-conductance Ca^{2+}-activated K^+ (BK) channels are pore-forming transmembrane proteins and are allosterically modulated by voltage and Ca^{2+} (1–5). The BKα subunits form tetramers, and both regulatory β- (6) and γ-subunits (7) can associate with the pore-forming α-subunits. Although the accessory subunits are not required for functional BK channels, they alter the sensitivity of the channels to Ca^{2+}, voltage, and various channel agonists. Uniquely for K^+ channels, each BKα subunit comprises seven transmembrane (S0–S6) domains, which contain voltage-sensing residues in S1–S4 (8–10) and the pore gate domain is located in S5–S6 (11). The transmembrane domain is attached to a large intracellular domain, which comprises two regulators of conductance for K^+ (RCK) domains (12). The RCK1 domain contains a high-affinity Ca^{2+}-binding site and a low-affinity cation-binding site, which senses Mg^{2+} and high concentrations of Ca^{2+} (13, 14). Another high-affinity Ca^{2+}-binding site, called the Ca^{2+} bowl (13–16), is found in the RCK2 domain. Ca^{2+} binding through these domains is transduced to the transmembrane domain via the S6/RCK1 linker (12, 17). Recent evidence (18) supports the idea that the cytosolic domain of this channel is responsible for sensing Ca^{2+}, because truncated BK channels lacking the C terminus are insensitive to Ca^{2+}.

BK channels play a number of important roles that govern the excitability of neuronal and smooth muscle cells. In bladder smooth muscle, for example, they contribute significantly to the repolarization phase of the action potential and thus modulate the contractile activity of this tissue (19). Interestingly, BKα knockout mice (20) display a functionally incontinent phenotype, presumably due to detrusor overactivity. Furthermore, a number of studies (21, 22) have suggested that the expression of BK channels is reduced in patients suffering from neurogenic detrusor overactivity. These results suggest that BK channel activators could represent a novel therapeutic approach for treating overactive bladder. However, despite the development of a large number of BK channel openers over the last two decades (23–29), they have failed to progress through clinical trials, because they showed poor efficacy, presumably due to their lack of effect at physiological membrane potentials, combined with a reduction in BK channels in patients with overactive bladder (30).

Recently, we synthesized a novel group of BK channel openers called the GoSlo-SR family (31). GoSlo-SR-5-6 (GoSlo) (10 μM) shifted the voltage dependence of activation in excess of −100 mV. Although the structure–activity relationships of these compounds has been established (31, 32), little is known about their mode of action on BK channels, other than GoSlo does not require the β_1-subunit to mediate its effects (33).

The purpose of the present study was to examine the molecular mechanisms underlying the excitatory effects of GoSlo on BK channels expressed in HEK cells. Recently, a number of studies have demonstrated that BK channel openers such as Cym04, NS1619, and omega-3 fatty acids mediate their effects, at least partially, through an interaction with the S6/RCK1 linker (34) or the S6 segment (35) of the BK channel. Our results demonstrate that GoSlo mediates its effects by interactions with S6 and the S4/S5 linker ($S4S5_L$), and this was reduced by combined 317, 326, and 227 mutations. The Horrigan–Aldrich (HA) allosteric model of BK channel gating (5) suggests that GoSlo enhanced the equilibrium constants for both pore opening and voltage sensor activation but reduced the voltage sensor/gate coupling.

Effects of GoSlo on Rabbit BKα Subunits Expressed in HEK Cells

We first examined the effects of GoSlo on inside-out patches of membrane from HEK cells expressing rabbit BK α-subunits (rWT). Fig. 1*A* shows control currents evoked from a holding

Significance

Large-conductance Ca^{2+}-activated K^+ (BK) calcium-activated potassium channels alter the excitability of a wide variety of cells including nerves and muscle. These channels are potential targets to treat diseases such as overactive bladder, hypertension, and erectile dysfunction. We have shown that a novel compound called GoSlo opens these channels and this effect is blocked when three mutations are introduced. The identification of this potential interaction site may permit the development of more potent, efficacious BK channel modulators to help treat the above diseases.

Author contributions: T.I.W., G.P.S., N.G.M., K.D.T., and M.A.H. designed research; T.I.W., A.S.K., R.J.L., A.M.A., and S.R. performed research; S.R. contributed new reagents/analytic tools; T.I.W., A.S.K., R.J.L., A.M.A., and M.A.H. analyzed data; and T.I.W., G.P.S., N.G.M., K.D.T., and M.A.H. wrote the paper.

Conflict of interest statement: S.R., G.P.S., N.G.M., K.D.T., and M.A.H. have submitted a patent application (IPN WO 2012/035122 A11) on this family of molecules.

*This Direct Submission article had a prearranged editor.

[1]T.I.W. and A.S.K. contributed equally to this work.

[2]To whom correspondence should be addressed. Email: mark.hollywood@dkit.ie.

This article contains supporting information online at www.pnas.org/lookup/suppl/doi:10.1073/pnas.1400555112/-/DCSupplemental.

potential of −60 mV through a range of potentials to +100 mV in 20-mV increments, before repolarizing to −80 mV. GoSlo (Fig. 1*B*, 10 μM, structure *Inset*) shifted the activation $V_{1/2}$ by more than −100 mV, decreased the activation time constant, and increased the deactivation time constant (Fig. S1). To quantify the effects of the drug on $V_{1/2}$, we plotted *GV* curves (Fig. 1*C*) from the *IV* relationship obtained in 100 nM Ca^{2+} in the absence and presence of GoSlo and compared its effects to increasing $[Ca^{2+}]_i$ to 1 and 10 μM Ca^{2+}. These data were fitted with the Boltzmann equation (solid lines), and in 13 experiments, summarized in Fig. 1*C*, GoSlo shifted the activation $V_{1/2}$ from 173 ± 2 to 50 ± 2 mV, which was similar to the effects of 1 μM Ca^{2+} ($V_{1/2}$ = 57 ± 3 mV; Fig. S1*C*). In the presence of 10 μM Ca^{2+}, the response to GoSlo was reduced ($\Delta V_{1/2}$ = −63 ± 6 mV; n = 7). In the absence of divalent cations in the pipette solution the Ca^{2+} sensitivity of the BK currents was higher than that reported in other studies (Fig. S2).

Functional Ca^{2+} or Mg^{2+} Sensors Not Required for GoSlo Effects

We first investigated the involvement of the two high-affinity Ca^{2+}-binding sites (Fig. 2*A*) on the GoSlo response. The Ca^{2+} and GoSlo responses of channels expressing mutations shown to reduce calcium binding at the RCK1 site, D367A (13), the RCK2 site, 5D5N (15, 16), or both sites, M513I:D898A (16), were recorded and compared with rWT (Fig. S1) and are summarized in Fig. 1*D*. Although the Ca^{2+} sensitivity of all mutants were reduced (Fig. S1*C*), the response to GoSlo was unaltered (Fig. 1*D*). Similarly, mutations of the Mg^{2+} sensors [E374A, E374A:E399N (36)] failed to reduce the response to GoSlo, suggesting that functional Ca^{2+} or Mg^{2+} sensors were not essential for its effects. We next deleted the C terminus of the BK channel [distal to residue 342 (18)] to narrow down the site for GoSlo interaction to the cytosolic or transmembrane domains. As recently demonstrated (18), these truncated channels were insensitive to Ca^{2+} (Fig. 1*E*), but were activated by GoSlo, which shifted activation $V_{1/2}$ more than −100 mV (Fig. 1*F*; n = 5). GoSlo effects were blocked by penitrem A (n = 8; Fig. S3).

Are S6/RCK1 Linkers Involved in the GoSlo Response?

Following the recent demonstration (34) that Cym04 and NS1619 open BK channels through interactions with the S6/RCK1 linker region (shown in orange in Fig. 2*A*), we examined the effects of GoSlo on the Slo1_9A splice variant. This contains an alternative exon 9, differing in 13 aa in the S6/RCK1 linker regions (37). Fig. 2*B* shows the amino acid sequence from residue 317 in the C-terminal half of S6 (S6C) to residue 342 at the distal end of the S6/RCK1 linker of BKα. This is designated 999 (34), because it contains the original exon 9, whereas the sequence of the Slo1_9a splice variant is designated AAA, which signifies alternative exon 9. The residues that differ between WT and Slo1_9a are represented in black. We first examined the effects of 10 μM GoSlo on the hWT channel and found that, in 100 nM Ca^{2+}, the $\Delta V_{1/2}$ was not significantly different (−104 ± 6 mV; n = 9) to that recorded in rWT or native rabbit bladder BK channels (31). Fig. 2*Di* shows typical currents evoked from hWT channels by a step to +100 mV in the presence of 100 nM Ca^{2+}, 10 μM Ca^{2+}, and 100 nM Ca^{2+} plus 10 μM GoSlo (blue trace), and is summarized in Fig. 2*Dii*. In contrast, the effects of 10 μM GoSlo were reduced in Slo1_9a (Fig. 2 *Ei* and *Eii*) where $\Delta V_{1/2}$ was −43 ± 6 mV (Fig. 2*C*; $P < 0.001$, ANOVA).

Given the reduction in the effect of GoSlo on Slo1_9a, we produced a series of chimeras in which S6C, the proximal linker, and the distal linker were independently exchanged between hWT and Slo1_9a (Fig. 2*B*). The Ca^{2+} sensitivity and effect of GoSlo on each chimera are shown in Fig. S4 *A* and *B*. When we compared the effect of GoSlo on these chimeras, a clear pattern was evident (Fig. 2*C*), in which the decrease in the effect of GoSlo was only dependent on the presence of the variant sequence (A) in the S6 segment (A99, $\Delta V_{1/2}$ = −53 ± 10 mV, n = 6, $P < 0.001$), regardless of whether the other regions were also altered (AA9, $\Delta V_{1/2}$ = −38 ± 5 mV, n = 6, $P < 0.001$; A9A, $\Delta V_{1/2}$ = −54 ± 10 mV, n = 6, $P < 0.001$). In contrast, the effect of NS1619 (30 μM; Fig. S4*C*) was unaffected in the A99 chimera but was reduced by ∼50% in the AA9 and 9A9 chimeras (34), consistent with the idea that the site of interaction of GoSlo with BK channels is different to NS1619.

We next examined the effects of mutating the three residues in S6 of the rWT channel that differ in Slo1_9a (S317, I323, and E324; Fig. 2*B*). Although the response to GoSlo was not significantly reduced in E324 or I323 mutants (Fig. 3 *B* and *C*), the S317R mutant was less responsive to GoSlo (Fig. 3*Ai*). This mutant activated with a $V_{1/2}$ of 200 ± 2 mV (Fig. 3*Aii*; n = 10), and in 10 μM GoSlo, the $\Delta V_{1/2}$ was −80 ± 8 mV (Fig. 3*C*). Interestingly, the response to GoSlo in the S317A mutant ($\Delta V_{1/2}$ = −115 ± 9 mV) was similar to rWT, suggesting that R317 altered either the efficacy or potency of GoSlo. When R317 was mutated back to S317, on the otherwise-unaltered Slo1_9a, the effects of

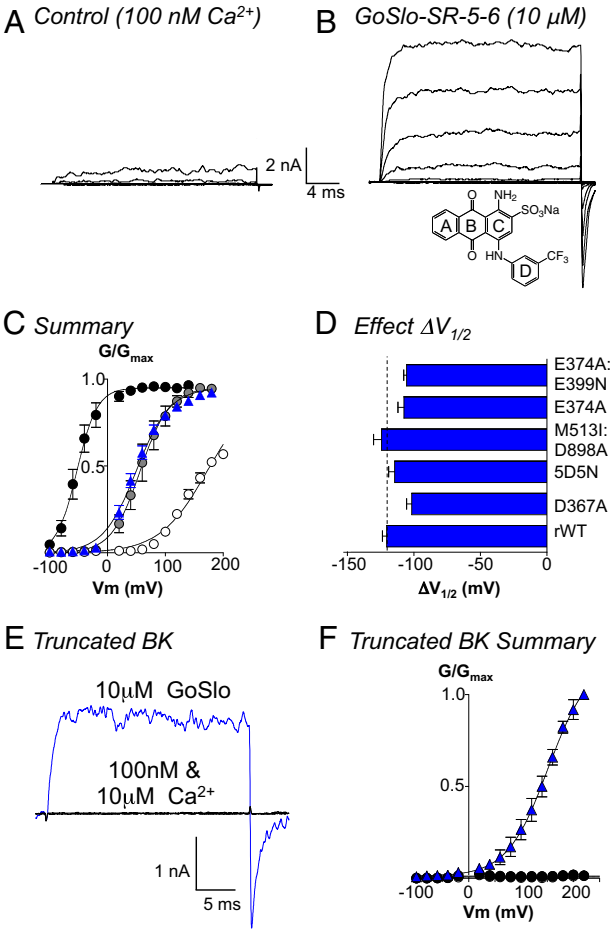

Fig. 1. GoSlo does not need functional Ca^{2+} or Mg^{2+} sensors. *A* shows currents evoked from −100 to +100 mV in 20-mV steps from a holding potential of −60 mV in 100 nM Ca^{2+}. (*B*) Currents evoked from the same patch following application of 10 μM GoSlo to the cytosolic face of the channel. GoSlo structure shown *Inset* in *B*. (*C*) Summary *GV* curves in 100 nM Ca^{2+} before (open circles) and during GoSlo (blue triangles), 1 μM Ca^{2+} (gray circles), and 10 μM Ca^{2+} (black circles), and solid lines show Boltzmann fits to the data. Data are quoted as the mean ± SEM (n = 13). (*D*) Mean $\Delta V_{1/2}$ (±SEM) of GoSlo obtained in a variety of mutants designed to reduce (D367A, n = 6; 5D5N, n = 5) or ablate (M513I:D898A, n = 6) Ca^{2+} or Mg^{2+} sensing (E374A, n = 7; E374A:E399N, n = 6). None of the mutants significantly reduced $\Delta V_{1/2}$. (*E*) The truncated BK construct [Slo1C-Kv-minT (18)] failed to evoke currents when depolarized to +100 mV and was insensitive to Ca^{2+} (black traces). Large currents were evoked in GoSlo (blue trace). (*F*) Summary *GV* curves for the truncated channel (n = 5) in the presence of 100 nM Ca^{2+} (white circles), 10 μM Ca^{2+} (black circles), and 10 μM GoSlo (blue triangles).

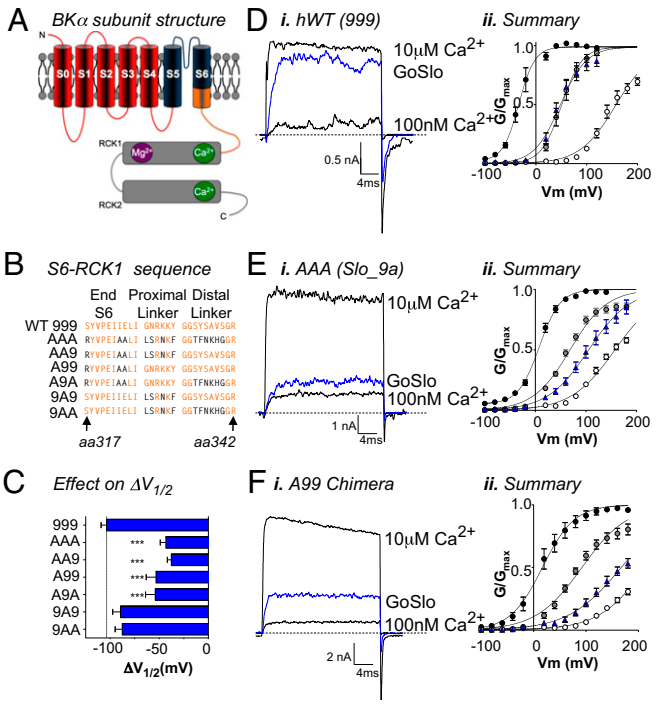

Fig. 2. Effects of GoSlo are reduced in Slo1_9a splice variants and chimeras. (*A*) Cartoon of a single BK α-subunit in which the transmembrane domains are labeled S0–S6 and the large intracellular cytosolic domain extends from the end of S6. The cytosolic region comprises two RCK domains containing a Mg^{2+} (purple) and two Ca^{2+} sensors (green). The cytosolic region is attached to the S6 segment via a linker, denoted in orange. The sequence of the orange region is shown in *B* for the human WT channel (designated 999, because it contains the normal exon 9) and the Slo1_9a splice variant (SV, designated AAA, because it contains an alternative exon 9). Differences in residues between these variants are shown in black text. Remaining sequences show the different chimeras used in this study. (*C*) Summary of the mean $\Delta V_{1/2}$ in response to application of GoSlo in 100 nM Ca^{2+}. The response to GoSlo was only significantly altered in the Slo1_9a splice variant ($n = 10$) and any chimera that contained the Slo1_9a S6 sequence ($n = 6$). *Di*, *Ei*, and *Fi* show the effects of GoSlo on currents evoked by a step to +100 mV in the presence of 10 μM Ca^{2+} (upper traces), 100 nM Ca^{2+} (lower traces), and in 10 μM GoSlo (blue traces) in human WT (*Di*; $n = 10$), Slo1_9a (*Ei*; $n = 10$), and the A99 chimera (*Fi*; $n = 6$), respectively. (*Dii–Fii*) Summary *GV* curves for the corresponding currents ($n = 6$–8), and the symbols have the same meaning as those in Fig. 1.

GoSlo were significantly restored, but mutation of either of the other two S6 residues in Slo1_9a had no significant effect (Fig. S5).

What Other Residues Are Involved in the Response to GoSlo?

Having established that the S317R mutation diminished the effect of GoSlo, we were interested in the location of S317 in the BK protein and potential interactions involving its side chain. Because the crystal structure of the transmembrane portion of the BK channel is unresolved, we used the structure of the Kv1.2/2.1 paddle-chimera (ref. 38; Protein Data Bank ID code 2R9R). We selected residues from regions in the 2R9R structure predicted to pack against L400, the equivalent residue to S317 in BK channels. Fig. 4*Ai* shows the 2R9R structure, with four color-coded α-subunits. The region within the white box is expanded (Fig. 4*Aii*), to show a portion of the channel in which subunits 2 and 4 are to the foreground. The residue number of 2R9R is shown along with the equivalent residue in the BK channel in parentheses. Marked in gray sticks are the only three residues from adjacent segments (L313, V406, F409) that were identified to be within the 4-Å cutoff of the L400 side chains. The equivalent residues from the BK channel are S317 (in S6C of subunit 2, colored in cyan), residues I323 and I326 in S6C of the adjacent α-subunit (subunit 4, shown in red), and residue L227 on the $S4S5_L$ of the adjacent subunit. We individually mutated each of these residues in rWT and examined the effects of GoSlo. The I323A mutant did not significantly affect the response to GoSlo (Fig. 3 *B* and *C*); however, the $\Delta V_{1/2}$ induced by GoSlo was reduced significantly in the L227A and I326A mutants (Fig. 4 *B–E*). It was further reduced in the double mutants S317R:I326A (Fig. 4*C*) and S317R:L227A, where the mean $\Delta V_{1/2}$ was reduced to −56 ± 4 and −65 ± 3 mV, respectively, in GoSlo ($P < 0.01$; Fig. 4*E*).

We also examined the effect of GoSlo on channels with the triple mutation L227A:S317R:I326A and compared these with rWT channels. In rWT, GoSlo produced a concentration-dependent enhancement of the current evoked by a step from −60 to +100 mV (Fig. 5*A*). Summary activation curves for each concentration of drug (300 nM to 30 μM) are shown in Fig. 5*B* ($n = 7$–12). The $\Delta V_{1/2}$ in each concentration of drug was plotted in Fig. 5*C* to yield an EC_{50} of ∼3 μM. Even though the Ca^{2+} sensitivity of the triple mutant was not decreased compared with rWT (Fig. S6*A*), it was much less responsive to GoSlo (Fig. 5 *D–F*) because the $\Delta V_{1/2}$ in 10 μM GoSlo was −15 ± 4 mV ($n = 11$). Due to the limited solubility of GoSlo, we were unable to obtain a full concentration effect curve (Fig. 5*F*), so it was unclear if potency or efficacy was reduced. Interestingly, the effects of NS1619 (30 μM) were unaltered in this mutant ($\Delta V_{1/2} = -40 \pm 3$ mV; $n = 5$) compared with rWT ($\Delta V_{1/2} = -42 \pm 3$ mV; $n = 6$).

Investigating the Molecular Mechanism of Action of GoSlo

We used the HA allosteric model (5) shown in Fig. 6*A* to help cast light on how GoSlo activated BK channels, as detailed in *SI Text*. As shown in Fig. 6*B*, the model can be simplified to sub-scheme 1 in the absence of Ca^{2+}. A typical record of single-channel currents obtained from a patch in the absence and presence of 10 μM GoSlo and in 1 μM Ca^{2+} is shown in Fig. 6*C*. Under control conditions, the open probability (P_O) decreased as the patch was hyperpolarized, but GoSlo increased P_O markedly, and was more effective than Ca^{2+} at these voltages. Fig. 6*E*

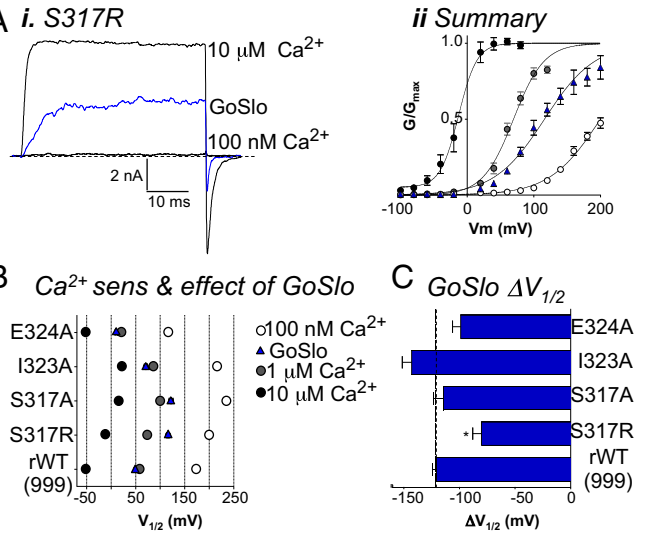

Fig. 3. The S317R mutant in the S6 segment reduces the effect of GoSlo. (*Ai*) Typical currents evoked in the S317R mutant by a step to +100 mV in 100 nM Ca^{2+} (lower trace), the presence of GoSlo (blue trace), and in 10 μM Ca^{2+} (upper trace). *Aii* shows the *GV* curves ($n = 10$) in 100 nM Ca^{2+} before (open circles) and during GoSlo application (blue triangles), 1 μM Ca^{2+} (gray circles), and 10 μM Ca^{2+} (black circles), and solid lines show Boltzmann fits to the data. (*B*) Plots of the mean activation $V_{1/2}$ for each S6 segment mutant in three different [Ca^{2+}] and in the presence of GoSlo. Colored symbols have the same meaning as in Fig. 1. (*C*) Mean $\Delta V_{1/2}$ obtained in 10 μM GoSlo in each of the mutants. The horizontal line shows the $\Delta V_{1/2}$ obtained in the rWT channel. Effect of GoSlo was only significantly reduced in the S317R mutant ($P < 0.05$, ANOVA).

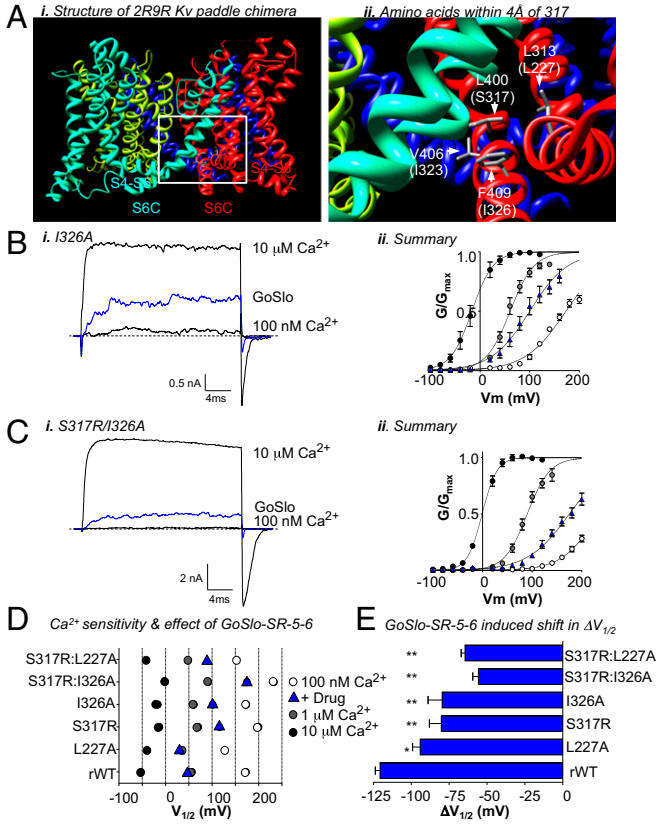

Fig. 4. Mutations in the S6C and S4S5$_L$ segments reduce the effect of GoSlo. (*Ai*) Structure of the Kv paddle chimera (2R9R) used to probe amino acids that may pack against S317 in the BK channel. Each of the four α-subunits are color coded. The area framed by the white box is expanded in *Aii*, which shows the three residues that are within 4 Å of L400 in the Kv structure. BK channel equivalent residues are shown in parentheses. S317 may protrude from the S6 segment marked in green, and the other residues are from the adjacent S6 segment and S4S5$_L$. (*Bi* and *Ci*) Typical currents evoked by a step to +100 mV in the absence and presence of GoSlo (blue traces) and in 10 μM Ca^{2+} (upper traces) in the I326A and S317R/I326A mutants, respectively. (*Bii* and *Cii*) *GV* curves (n = 6) in 100 nM Ca^{2+} before (open circles) and during GoSlo application (blue triangles), 1 μM Ca^{2+} (gray circles), and 10 μM Ca^{2+} (black circles) in the I326A and S317R/I326A mutants, respectively. Solid lines show Boltzmann fits to the data. (*D*) Plot of the activation $V_{1/2}$ for each mutant in three different [Ca^{2+}] and GoSlo. The colored symbols have the same meaning as in *Bii*. (*E*) Mean $\Delta V_{1/2}$ obtained in response to application of 10 μM GoSlo in each of the mutants (n = 5–7).

shows summary P_O–V relationships in which GoSlo enhanced P_O at all voltages, but its effects were greatest at negative potentials. For example at −140 mV, P_O increased ∼1,700-fold, whereas application of 1 μM Ca^{2+} only enhanced P_O 33-fold. These data were fitted with the HA model (Eq. **S3**) to yield the solid lines in Fig. 6*E*, and the values obtained by these fits are summarized in Table S1. In GoSlo, there was little change in Z_J, but the charge associated with pore opening (Z_L) was reduced to 0.18e, as evidenced by the reduced voltage sensitivity of the C–O transition at positive potentials (Fig. S7*C*). Both L_0 (700-fold) and J_0 (eightfold) were significantly increased, whereas the allosteric coupling factor D was reduced by ∼60%, suggesting that GoSlo mediates it effects predominantly by shifting the C–O equilibrium to stabilize the open state (↑L_0) and also stabilizes voltage sensor activation (↑J_0). If GoSlo activates the voltage sensors and decouples them from channel opening, a very specific series of changes should be observed in mean activation charge displacement vs. voltage (Qa–V) relationship. Thus, the peak Qa amplitude (Qa_{MAX}) and its width would be reduced as a consequence of ↓D (10) and the Qa–V relationship should be shifted negatively, due to the shift in the R–A equilibrium. Fig. 6*G* shows a Qa–V plot calculated from the logarithmic slope of the P_O–V data (39), fitted with Eq. **S6**, and suggests that all three predictions held.

When we repeated these experiments on the triple mutant, GoSlo only modestly increased P_O (Fig. 6*D*). As shown in Fig. 6*F*, when the summary P_O–V data were fitted with the HA equation, the mutant channels appeared similar to the WT, although the allosteric coupling factor (D) was ∼20% smaller compared with WT. In GoSlo, P_O only increased ∼15-fold at negative potentials, but D was reduced from 11 ± 0.3 to 7 ± 0.1 and J_0 increased from 0.08 to 0.17 in GoSlo. As Fig. 6*H* suggests, the mutant Qa_{MAX} was smaller than WT, consistent with the reduction in D. In the presence of GoSlo, Qa_{MAX} was reduced further and the Qa–V relationship was narrower, as expected with a further reduction in D. However, the hyperpolarizing shift in the Qa–V relationship was decreased (Table S2), consistent with a reduced shift in voltage sensor activation.

Discussion

The results presented suggest that the effects of GoSlo (*i*) do not require functional Ca^{2+}- or Mg^{2+}-binding sites, (*ii*) remain when the cytosolic domain of the channel is deleted, (*iii*) are significantly reduced in the Slo1_9a splice variant, (*iv*) are reduced in the S6C mutants S317R and I326A, (*v*) are decreased in the S4S5$_L$ mutant L227A, (*vi*) are ablated in the S4S5$_L$/S6 triple mutant, and (*vii*) are mediated predominantly by shifting the

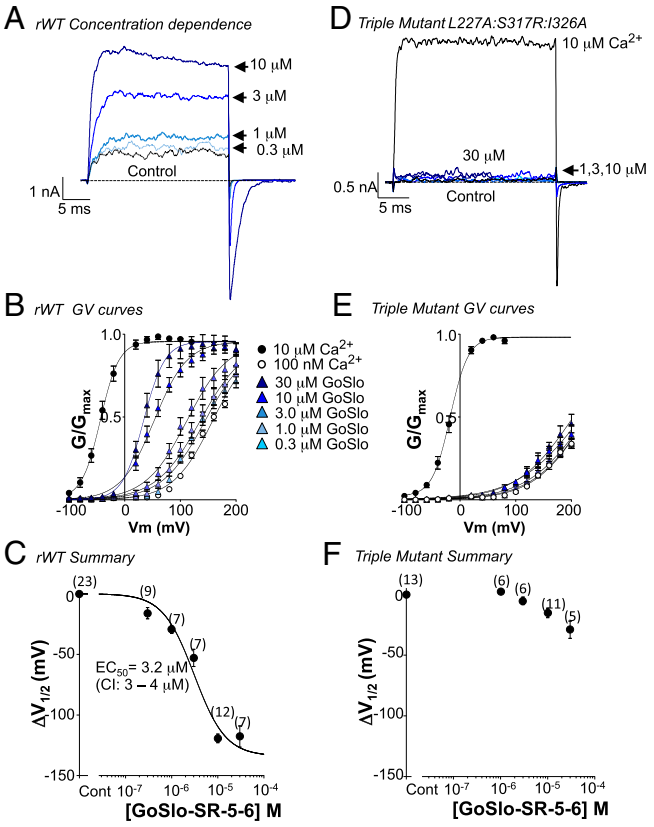

Fig. 5. The triple mutant practically abolishes the response to GoSlo. Currents from rWT (*A*) and the triple mutant (*D*) were evoked by a step to +100 mV in the absence (black trace) and presence of increasing concentrations of drug (blue traces). The concentration dependence of the currents to GoSlo in the rWT (*B*) and triple mutant (*E*) was assessed from −100 to +200 mV to generate the respective *GV* curves. The $\Delta V_{1/2}$ in each [drug] was plotted in *C* and fitted with the Langmuir equation to yield an EC_{50} of 3.2 μM for the rWT. We were unable to obtain a full concentration effect curve in this mutant, although the efficacy of the drug appears reduced compared with rWT (*F*). Numbers in parentheses represent the number of replicates.

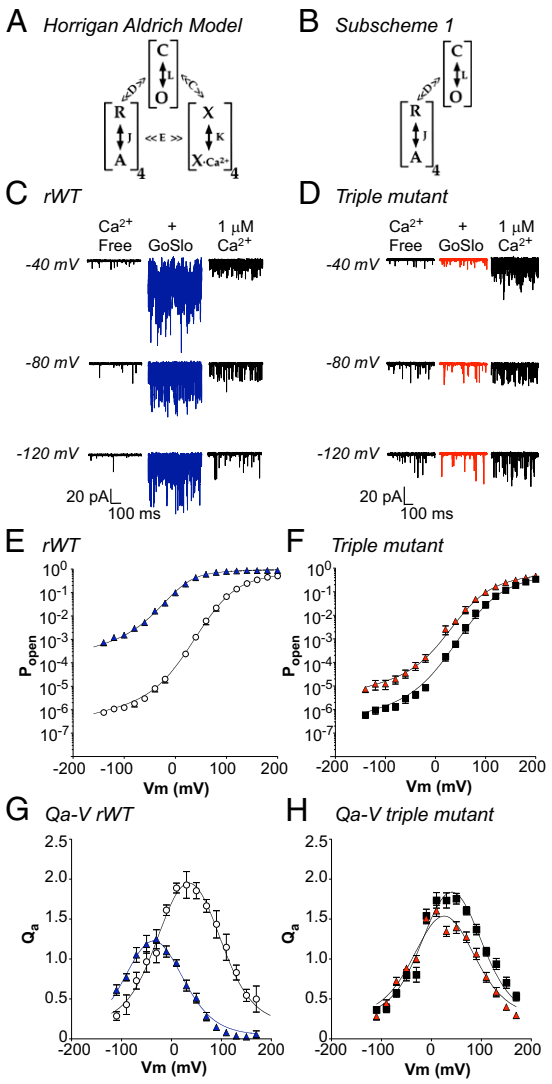

Fig. 6. Using the HA model to assess the molecular mechanisms of action of GoSlo. (*A*) The HA model in which C and O represent the closed and open states of the channel and is governed by the equilibrium constant L. R and A represent the resting and activated states of each of the four voltage sensors and is governed by the equilibrium constant J. X and $X_{Ca}{}^{2+}$ are the unbound and bound states of the Ca^{2+} sensors, respectively, and K is the equilibrium constant. C and E represent the allosteric factors that couple Ca^{2+} binding to channel opening and voltage sensor activation, respectively, and allosteric factor *D* couples channel opening and voltage sensor activation. (*B*) HA model applicable in the absence of Ca^{2+}. (*C*, *E*, and *G*) Typical records and summary data from rWT BK channels. *D*, *F*, and *H* show experiments with the triple (L227A:I326A:317R) mutant. *C* shows single-channel currents from a WT patch containing 180 channels and held at –40, –80, and –120 mV in the absence of Ca^{2+} (left traces), the presence of GoSlo (middle traces), and 1 μM Ca^{2+} (right trace). GoSlo was more effective at increasing the P_O than Ca^{2+} at negative voltages. Summary data in *E* shows mean P_O–*V* relationships in the absence (open circles) and presence (blue triangles) of GoSlo (10 μM). Solid lines are fits obtained with Eq. **S3**, which yielded $L_0 = 3.7 \times 10^{-6}$, $Z_L = 0.28$, $J_0 = 0.09$, $Z_J = 0.73$, and $D = 13.8$ before, and $L_0 = 2.5 \times 10^{-3}$, $Z_L = 0.28$, $J_0 = 0.7$, $Z_J = 0.71$, and $D = 5$ in GoSlo. (*G*) Mean *Qa*–*V* relationship for rWT, where Qa_{MAX} was 1.95 ± 0.14 at 30 mV in control compared with 1.17 ± 0.13 in GoSlo. (*D*) Currents from a patch containing 350 triple mutant channels in the absence (*Left*), presence of GoSlo (*Middle*) and 1 μM Ca^{2+} (*Right*). *F* shows P_O in triple mutant before (black squares) and during GoSlo (red triangles). Solid lines are fits obtained with Eq. **S3**, where $L_0 = 3.6 \times 10^{-6}$, $Z_L = 0.3$e, $J_0 = 0.08$, $Z_J = 0.7$, and $D = 11$ in control, and $L_0 = 3.9 \times 10^{-5}$, $Z_L = 0.28$, $J_0 = 0.17$, $Z_J = 0.69$, and $D = 7$ in GoSlo (red triangles). (*H*) Mean *Qa*–*V* relationship of the mutant before (black squares) and during GoSlo (red triangles), where Qa_{MAX} was reduced from 1.76 ± 0.07 at +50 mV to 1.4 ± 0.07 at +50 mV. Solid lines represent fits to the data using Eq. **S6** and yielding the values quoted in Table S2.

pore-gating equilibrium (L_0) toward the open state. These results support the idea that GoSlo mediates its effects through an interaction with residues in the transmembrane domain of the channel.

Over the last few years, a number of studies have examined the molecular mechanisms underlying the excitatory effects of different BK channel modulators (34, 35). A recent study (34) showed that Cym04 and NS1619 were less effective at opening Slo1_9a splice variant BK channels and provided evidence to support a role of residue K330 in the proximal linker in mediating the response to these compounds. The results from the present study suggest that, although the effects of GoSlo are significantly attenuated in the Slo1_9a splice variant, they were only slightly reduced in chimeras containing the sequence for Slo1_9a in either the proximal or distal linkers (9AA, 9A9). In keeping with previous reports (34), the $\Delta V_{1/2}$ induced by NS1619 was reduced ~50% in chimeras containing the Slo1_9a proximal linker sequence (9A9, AA9). The effect of NS1619 was not altered in the A99 chimera containing the S6C sequence from the splice variant (Fig. S4*C*). In contrast, the effects of GoSlo were significantly reduced in all chimeras possessing the Slo1_9a S6C segment. Our results suggest that the presence of R317 in the splice variant accounts for a significant proportion of the reduced effect, because the responsiveness of the Slo1_9a channels to GoSlo was partially restored when the arginine was mutated back to serine (Fig. S5). The involvement of S317 is certainly unexpected, because one interpretation of cysteine modification experiments (40) suggests that it may face into the pore in the open channel (and thus is shifted in position relative to K_v channels). If so, the side chain of S317 would only be available to interact with GoSlo in the closed state. The fact that the S317A mutant did not reduce the effect of GoSlo may suggest that the S317R mutation is not involved directly in the binding of GoSlo, but interferes with its binding to other, unidentified residues. Alternatively, GoSlo may interact with backbone of S317, and this may be inaccessible to GoSlo in the S317R mutant.

Having established that the substitution S317R diminished the GoSlo effect, we used the 2R9R crystal structure (38) to identify residues whose side chains may interact with the side chain of residue 317. Although the applicability of the 2R9R model to BK structure has been questioned, we were able to identify three residues, which, when mutated together, ablated the response to GoSlo. As Fig. 4*Aii* suggests, the corresponding residues in the BK channel predicted to pack against the side chain of 317 are I323 and I326, in S6C, and L227, in the $S4S5_L$, all three of which are in an adjacent subunit. Both I326A and L227A mutants were significantly less sensitive to GoSlo, the effects of GoSlo were further reduced (~50%) in the double mutants (S317R:L227A; S317R:I326A) and almost abolished in the triple mutant, where the $\Delta V_{1/2}$ was reduced by >80%. Interestingly neither the effects of increasing Ca^{2+} or NS1619 were reduced in this mutant, suggesting that it selectively ablates the response to GoSlo.

We examined the molecular mechanisms of GoSlo using the HA allosteric gating model (5) and found that the effects of GoSlo could be modeled by enhancing L_0 ~700-fold, J_0 ~8-fold, and reducing the allosteric coupling factor *D* by ~60%. Thus, it appears that GoSlo activated the channels primarily by shifting the C–O equilibrium toward the open state. In addition, GoSlo shifted the activation of the voltage sensors ($\Delta V_{HC} \sim -70$ mV; Eq. **S7**) but had little effect on the charge associated with voltage sensor movement (Z_J). However, it did appear to reduce the voltage sensitivity of the C–O transition, as evidenced by the reduction in Z_P (Fig. S7), perhaps suggesting that, in GoSlo, when the voltage sensors are maximally activated, the C–O transition is less voltage sensitive (Fig. S8). Although GoSlo appeared to activate the voltage sensors, it is interesting to note that it also reduced coupling between them and the pore, as evidenced by (*i*) the reduced amplitude of Qa_{MAX} in drug and (*ii*) the narrowing of the *Qa*–*V* curve relative to control. In the triple mutant, the *D* factor was reduced compared with WT, and interestingly, the kinetics of activation were both slower (Fig. S7*B*)

and less voltage dependent (Fig. S7*D*, filled squares) than the WT channel. It appears from our data that the voltage sensor gating charge of this mutant is unaltered (Table S1) and that the voltage sensors can activate, as evidenced by the similarity in shape of the P_O–V (Fig. 6) relationship in WT and the triple mutant. A potential explanation for the reduction in the activation kinetics is that voltage sensor activation is significantly slowed in this mutant, but this will require confirmation by recording gating currents.

Our working hypothesis to explain the molecular mechanism of action of GoSlo is that the bulky D ring of GoSlo inserts into a hydrophobic pocket between the $S4S5_L$ and S6C and perturbs the interaction between these two regions, resulting in channel opening, voltage sensor activation, and reduced coupling between the voltage sensor and the gate. Reductions in hydrophobic interactions in this region certainly appear to enhance BK channel activity, because the loss of the aliphatic side chain in the L227A mutant significantly left shifted the *GV* relationship in 100 nM Ca^{2+} compared with rWT (Fig. 4*D*), as recently suggested (41). This may also help to explain the observation that increasing D ring diameter enhances the efficacy of GoSlo compounds (32), perhaps as a result of forcing $S4S5_L$ and S6C apart.

In conclusion, the results of this study demonstrate that GoSlo is an efficacious BK channel opener that appears to interact with residues in the $S4S5_L$ and S6C segments to promote channel opening, primarily by stabilizing both the open state of the channel and the activated state of the voltage sensors.

Materials and Methods

Experiments were performed on BKα subunits expressed in HEK cells and studied with the inside-out configuration of the patch-clamp technique. The concentrations of Ca^{2+} in each experiment applied to the cytosolic face of the channel are shown in each figure. Standard molecular biology methods were used for mutagenesis (42) and chimera generation. The HA model (5) was used to elucidate the molecular mechanism. See *SI Materials and Methods* for details. Data are expressed as the mean ± SEM.

ACKNOWLEDGMENTS. We thank C. Lingle, L. Salkoff, R. Aldrich, and F. Horrigan for useful discussions. This work was funded by a Science Foundation Ireland Research Frontiers Programme Award (11/RFP/BMT/3143). S.R. and T.I.W. were funded through the Enterprise Ireland Applied Research Enhancement Scheme. A.M.A. was funded by Dundalk Institute of Technology Research Office.

1. Barrett JN, Magleby KL, Pallotta BS (1982) Properties of single calcium-activated potassium channels in cultured rat muscle. *J Physiol* 331:211–230.
2. Moczydlowski E, Latorre R (1983) Gating kinetics of Ca^{2+}-activated K^+ channels from rat muscle incorporated into planar lipid bilayers. Evidence for two voltage-dependent Ca^{2+} binding reactions. *J Gen Physiol* 82(4):511–542.
3. Cui J, Cox DH, Aldrich RW (1997) Intrinsic voltage dependence and Ca^{2+} regulation of mslo large conductance Ca-activated K^+ channels. *J Gen Physiol* 109(5):647–673.
4. Cox DH, Cui J, Aldrich RW (1997) Allosteric gating of a large conductance Ca-activated K^+ channel. *J Gen Physiol* 110(3):257–281.
5. Horrigan FT, Aldrich RW (2002) Coupling between voltage sensor activation, Ca^{2+} binding and channel opening in large conductance (BK) potassium channels. *J Gen Physiol* 120(3):267–305.
6. Brenner R, Jegla TJ, Wickenden A, Liu Y, Aldrich RW (2000) Cloning and functional characterization of novel large conductance calcium-activated potassium channel β subunits, hKCNMB3 and hKCNMB4. *J Biol Chem* 275(9):6453–6461.
7. Yan J, Aldrich RW (2010) LRRC26 auxiliary protein allows BK channel activation at resting voltage without calcium. *Nature* 466(7305):513–516.
8. Díaz L, et al. (1998) Role of the S4 segment in a voltage-dependent calcium-sensitive potassium (hSlo) channel. *J Biol Chem* 273(49):32430–32436.
9. Cui J, Aldrich RW (2000) Allosteric linkage between voltage and Ca^{2+}-dependent activation of BK-type mslo1 K^+ channels. *Biochemistry* 39(50):15612–15619.
10. Ma Z, Lou XJ, Horrigan FT (2006) Role of charged residues in the S1-S4 voltage sensor of BK channels. *J Gen Physiol* 127(3):309–328.
11. Yellen G (2002) The voltage-gated potassium channels and their relatives. *Nature* 419(6902):35–42.
12. Jiang Y, et al. (2002) Crystal structure and mechanism of a calcium-gated potassium channel. *Nature* 417(6888):515–522.
13. Xia XM, Zeng X, Lingle CJ (2002) Multiple regulatory sites in large-conductance calcium-activated potassium channels. *Nature* 418(6900):880–884.
14. Zeng XH, Xia XM, Lingle CJ (2005) Divalent cation sensitivity of BK channel activation supports the existence of three distinct binding sites. *J Gen Physiol* 125(3):273–286.
15. Schreiber M, Salkoff L (1997) A novel calcium-sensing domain in the BK channel. *Biophys J* 73(3):1355–1363.
16. Bao L, Kaldany C, Holmstrand EC, Cox DH (2004) Mapping the BKCa channel's "Ca^{2+} bowl": Side-chains essential for Ca^{2+} sensing. *J Gen Physiol* 123(5):475–489.
17. Niu X, Qian X, Magleby KL (2004) Linker-gating ring complex as passive spring and Ca^{2+}-dependent machine for a voltage- and Ca^{2+}-activated potassium channel. *Neuron* 42(5):745–756.
18. Budelli G, Geng Y, Butler A, Magleby KL, Salkoff L (2013) Properties of Slo1 K^+ channels with and without the gating ring. *Proc Natl Acad Sci USA* 110(41):16657–16662.
19. Imaizumi Y, et al. (1998) Ca^{2+} images and K^+ current during depolarization in smooth muscle cells of the guinea-pig vas deferens and urinary bladder. *J Physiol* 510(Pt 3):705–719.
20. Meredith AL, Thorneloe KS, Werner ME, Nelson MT, Aldrich RW (2004) Overactive bladder and incontinence in the absence of the BK large conductance Ca^{2+}-activated K^+ channel. *J Biol Chem* 279(35):36746–36752.
21. Hristov KL, et al. (2013) Neurogenic detrusor overactivity is associated with decreased expression and function of the large conductance voltage- and Ca^{2+}-activated K^+ channels. *PLoS One* 8(7):e68052.
22. Chang S, et al. (2010) Detrusor overactivity is associated with downregulation of large-conductance calcium- and voltage-activated potassium channel protein. *Am J Physiol Renal Physiol* 298(6):F1416–F1423.
23. Strøbaek D, et al. (1996) Modulation of the Ca^{2+}-dependent K^+ channel, hslo, by the substituted diphenylurea NS 1608, paxilline and internal Ca^{2+}. *Neuropharmacology* 35(7):903–914.
24. Argentieri TM, Butera JA (2006) An overview of potassium channel activators for the treatment of overactive bladder: a survey of new structures 2000–2005. *Expert Opin Ther Pat* 16(5):573–585.
25. Nardi A, Calderone V, Olesen SP (2006) Potassium channel openers: The case of BK channel activators. *Lett Drug Des Discov* 3:210–218.
26. Garcia ML, Shen DM, Kaczorowski GJ (2007) High-conductance calcium-activated potassium channels: Validated targets for smooth muscle relaxants? *Expert Opin Ther Pat* 17:831–842.
27. Nardi A, Olesen SP (2007) Acrylamides as potassium channel openers. *Expert Opin Ther Pat* 17(10):1215–1226.
28. Bentzen BH, et al. (2007) The small molecule NS11021 is a potent and specific activator of Ca^{2+}-activated big-conductance K^+ channels. *Mol Pharmacol* 72(4):1033–1044.
29. Nardi A, Olesen SP (2008) BK channel modulators: A comprehensive overview. *Curr Med Chem* 15(11):1126–1146.
30. Oger S, et al. (2011) Effects of potassium channel modulators on myogenic spontaneous phasic contractile activity in human detrusor from neurogenic patients. *BJU Int* 108(4):604–611.
31. Roy S, et al. (2012) Structure-activity relationships of a novel group of large-conductance Ca^{2+}-activated K^+ (BK) channel modulators: The GoSlo-SR family. *ChemMedChem* 7(10):1763–1769.
32. Roy S, et al. (2014) Development of GoSlo-SR-5-69, a potent activator of large conductance Ca^{2+}-activated K^+ (BK) channels. *Eur J Med Chem* 75:426–437.
33. Large RJ, et al. (2015) Effects of the novel BK channel opener GoSlo-SR-5-130 are dependent on the presence of BK_β subunits. *Brit J Pharmacol*, 10.1111/bph.13085.
34. Gessner G, et al. (2012) Molecular mechanism of pharmacological activation of BK channels. *Proc Natl Acad Sci USA* 109(9):3552–3557.
35. Hoshi T, Xu R, Hou S, Heinemann SH, Tian Y (2013) A point mutation in the human Slo1 channel that impairs its sensitivity to omega-3 docosahexaenoic acid. *J Gen Physiol* 142(5):507–522.
36. Yang H, et al. (2008) Activation of Slo1 BK channels by Mg^{2+} coordinated between the voltage sensor and RCK1 domains. *Nat Struct Mol Biol* 15(11):1152–1159.
37. Soom M, Gessner G, Heuer H, Hoshi T, Heinemann SH (2008) A mutually exclusive alternative exon of slo1 codes for a neuronal BK channel with altered function. *Channels (Austin)* 2(4):278–282.
38. Long SB, Campbell EB, Mackinnon R (2005) Crystal structure of a mammalian voltage-dependent Shaker family K^+ channel. *Science* 309(5736):897–903.
39. Sigg D, Bezanilla F (1997) Total charge movement per channel. The relation between gating charge displacement and the voltage sensitivity of activation. *J Gen Physiol* 109(1):27–39.
40. Zhou Y, Xia XM, Lingle CJ (2011) Cysteine scanning and modification reveal major differences between BK channels and Kv channels in the inner pore region. *Proc Natl Acad Sci USA* 108(29):12161–12166.
41. Sun L, Adhikari S, Zou S, Horrigan FT (2012) The interaction of voltage-sensor and gate in BK channels. *Biophys J* 102(3):684a.
42. Sawano A, Miyawaki A (2000) Directed evolution of green fluorescent protein by a new versatile PCR strategy for site-directed and semi-random mutagenesis. *Nucleic Acids Res* 28(16):E78.